ISSN 1573-160X, *PHYSICAL OCEANOGRAPHY*, Vol. 33, Iss. 4, pp. 650-674 (2026)
Original Russian Text © The Authors, 2026,
published in *Morskoy Gidrofizicheskiy Zhurnal*, 2026, Vol. 42, Iss. 4, pp. 628–653

Original article

Light Absorption by Main Optically Active Components in Shelf Waters of the Kamchatka Peninsula (August–September 2023). Part 1. Phytoplankton

T. Ya. Churilova [1, 2, ✉], E. Yu. Skorokhod [1, 2], N. A. Moiseeva [1], A. S. Buchelnikov [1, 3], T. V. Efimova [1, 2], P. A. Salyuk [4], A. V. Yatsuk [5]

[1] *A. O. Kovalevsky Institute of Biology of the Southern Seas of Russian Academy of Sciences, Sevastopol, Russian Federation*
[2] *Far Eastern Federal University, Vladivostok, Russian Federation*
[3] *Sevastopol State University, Sevastopol, Russian Federation*
[4] *V. I. Il'ichev Pacific Oceanological Institute, Far Eastern Branch of Russian Academy of Sciences, Vladivostok, Russian Federation*
[5] *Sirius University of Science and Technology, Sirius, Russian Federation*
✉ *tanya.churilova@gmail.com*

Abstract
Purpose. The purpose of the study is to analyse the spatial variability of chlorophyll *a* concentration (*TChl-a*) and spectral coefficients of light absorption by phytoplankton ($a_{\text{ph}}(\lambda)$), as well as to determine the relationship between $a_{\text{ph}}(\lambda)$ and *TChl-a* in the wavelength range from 400 to 700 nm at 2 nm intervals for different layers of the euphotic zone.
Methods and Results. The research was carried out at 79 stations in August–September 2023. Water samples were collected using Niskin bottles, chlorophyll *a* concentration was determined spectrophotometrically, and spectral absorption coefficients were measured on moistened glass fiber filters using an integrating sphere. The vertical structure was analysed based on the CTD data, chlorophyll *a* fluorescence, and photosynthetically available radiation (PAR). The upper mixed layer (UML) and the underlying layers down to the depths with 1 and 0.1% of PAR were identified. The parameterisation was performed using a power function $a_{\text{ph}}(\lambda) = A(\lambda) \cdot TChl\text{-}a^{B(\lambda)}$ for two layers of the euphotic zone and the underlying layer. *TChl-a* in the surface layer varied within 0.7–14 mg·m^{-3} in the Pacific Ocean and within 0.87–8.9 mg·m^{-3} in the Sea of Okhotsk. Four types were identified. Their formation resulted from water stratification, its location within the euphotic zone and nutrient supply. The coefficients *A*(438) and *A*(675) were 0.058 and 0.023 m^2·mg^{-1} for the UML, and 0.043 and 0.020 m^2·mg^{-1} for the layer between UML and the bottom of the euphotic zone. It was shown that at the same light intensity, the chlorophyll *a*-specific absorption coefficient $a^*_{\text{ph}}(\lambda)$ decreased with increasing *TChl-a,* which was related to the stronger pigment package effect as the proportion of large-celled species in phytoplankton increased.
Conclusions. For the first time, parameterisation of light absorption by phytoplankton for the study area was performed within the 400–700 nm range (at 2 nm intervals) for two layers in the euphotic zone and for the underlying one. Statistically significant differences between the parameterisation coefficients of these layers were revealed. The obtained relationships can be used to retrieve the $a_{\text{ph}}(\lambda)$ spectra from *TChl-a*, which is necessary for assessing the photosynthetic characteristics of phytoplankton and determining primary production using the spectral method, as well as for developing regional satellite algorithms and operational monitoring of water productivity off the Kamchatka Peninsula.

Keywords*:* chlorophyll, spectral light absorption coefficient, phytoplankton, shelf waters, Kamchatka

Acknowledgements: During the scientific cruise, water samples were taken within the framework of scientific and educational programme "Floating University" (agreement No. 075-01593-23-06); data processing and primary analysis of the effects of environmental factors on the chlorophyll *a* concentration were performed within the framework of state assignment of FRC IBSS

No. 124030100106-2; vertical profiles of chlorophyll *a* fluorescence were measured within the framework of state assignment of POI FEB of RAS No. 124022100080-0; and the study of variability of bio-optical properties was funded by the Ministry of Science and Higher Education of the Russian Federation, project No. FZNS-2024-0037.

For citation: Churilova, T.Ya., Skorokhod, E.Yu., Moiseeva, N.A., Buchelnikov, A.S., Efimova, T.V., Salyuk, P.A. and Yatsuk, A.V., 2026. Light Absorption by Main Optically Active Components in Shelf Waters of the Kamchatka Peninsula (August–September 2023). Part 1. Phytoplankton. *Physical Oceanography*, 33(4), pp. 650-674.

Introduction

The Sea of Okhotsk (SO) and the north-western Pacific Ocean (PO) are among the most biologically productive regions in the global ocean [1] [1–4]. In the southern SO, spring "bloom" of phytoplankton and high productivity [5–9] are due to the availability of nutrients [6]. In the productive north-western part of the PO, off the southeast coast of the Kamchatka Peninsula [4, 10], an analysis of satellite data from 2002 to 2020 [11] showed a regular increase in chlorophyll *a* concentration (phytoplankton "bloom") in late September – early October. In years with intense "bloom", high chlorophyll-*a* concentrations were observed not only in coastal waters with intensive river runoff, but also in shelf and continental slope areas, which was associated with an abnormal increase in temperature and influx from deeper sea layers due to mixing caused by the passage of cyclones over this area [11]. The highest concentrations of chlorophyll *a* were observed in the coastal waters of Avacha Bay [11], which was due to the influx of nutrients mainly of volcanic origin from coastal and river runoff [12, 13], as well as the influence of biogeochemical and hydrological factors during the period of maximum water warming [14].

Intense phytoplankton "bloom" can be dangerous for the ecosystem. Harmful algal "blooms" (HABs) were observed in the coastal waters both in the SO and the PO near the Kamchatka Peninsula [15–17]. In the autumn of 2020, the intensive HAB off the coasts of the Kamchatka Peninsula caused catastrophic damage to marine life and health problems for humans [17]. In this regard, an operational monitoring system using remote sensing capabilities is of particular relevance. The unique capabilities of satellite oceanography [18] make it possible to track anomalies in real time. However, chlorophyll *a* concentrations in the SO in the summer of 2006 retrieved using the *OC*4v6 (SeaWiFS) and the *OC*3*M* (MODIS) algorithms were overestimated by factors of 2.6 and 3.6 [19]. In the coastal waters of the PO (in Avacha Bay) in the summer of 2017, the inaccuracy of satellite data was also demonstrated [20].

The problem of accuracy of satellite estimates in optically complex waters [21–23], which include almost all coastal waters, could be solved by developing regional algorithms based on bio-optical properties of this region. Variability of light

[1] North Pacific Marine Science Organization (PICES), 2009. *PICES Annual Report 2009: Eighteenth Annual Meeting*. Jeju, Korea, October 23–November 1, 2009. Sidney, British Columbia, Canada: PICES, 273 p.

absorption by phytoplankton was studied in the south-western SO in the summer of 2006 [19]. However, the relationship between phytoplankton light absorption coefficient ($a_{\mathrm{ph}}(\lambda)$) and concentration of chlorophyll *a* plus phaeopigments (*TChl-a*) was not revealed. This parameterisation is necessary for a correct assessment of *TChl-a* from $a_{\mathrm{ph}}(\lambda)$ retrieved using a bio-optical satellite algorithm, specifically a three-band algorithm [24].

The aim of this study is to analyse the spatial distribution of *TChl-a* and the spectral coefficient $a_{\mathrm{ph}}(\lambda)$ and their dependence on environmental factors, and to parameterise the $a_{\mathrm{ph}}(\lambda)$ vs *TChl-a* relationship for the visible domain (400–700 nm) with high spectral resolution for different layers of the euphotic zone.

Materials and methods

The study was conducted in the shelf waters of the PO and SO near the southern part of the Kamchatka Peninsula during an expedition on the RV *Professor Multanovsky* from 15 August to 20 September 2023 (Fig. 1). Water samples were collected using 10-litre Niskin bottles mounted on a CTD system (Sea-Bird) measuring hydrophysical characteristics (temperature, salinity, water density). The sampling depths were determined based on the vertical distribution of hydrophysical parameters and chlorophyll *a* fluorescence measured using a submersible fluorometer (WetStar, W535-1246).

Samples (1–2 L) for the analysis of photosynthetic pigment concentrations were filtered onto 25 mm diameter glass fibre filters (GF/F, Whatman) under low vacuum pressure (< 25 hPa). Filters were stored in a dewar with liquid nitrogen until analysis. For the pigment extraction, a two-step method was used: the pigments were extracted with 90% acetone (5 ml) using a vibro-homogenizer, and then the extract was clarified by centrifugation. The procedure was repeated: the extract was poured off and another 5 ml of 90% acetone was added to the residue. Concentrations of chlorophyll *a* and phaeopigments were determined spectrophotometrically [25, 26].

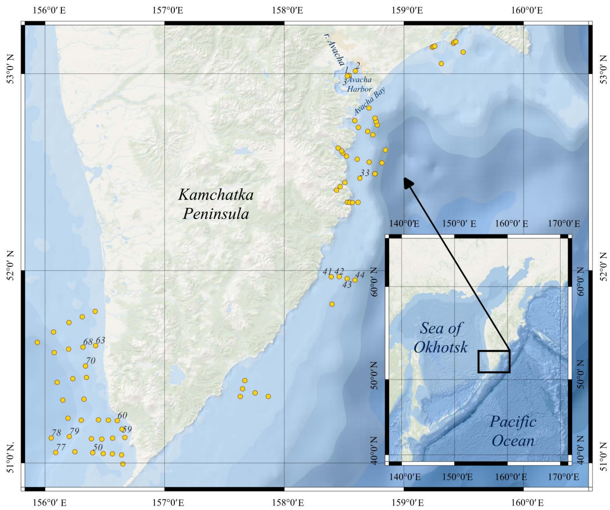

F i g. 1. The southern part of the Kamchatka Peninsula with a scheme of station locations in August–September 2023. The inset shows the region of the Sea of Okhotsk and the north-western Pacific Ocean, with the study area outlined by a rectangular contour

The spectral absorption coefficient of phytoplankton was determined by the "Quantitative Filter Technique" [27, 28] in line with the protocol [2]. Samples were filtered onto GF/F filters (Whatman) under low vacuum (< 25 hPa). The filters were stored in liquid nitrogen until analysis. The optical density (OD) of the particles (collected on the filter) was measured from 350 to 750 nm at 1-nm resolution using a Perkin Elmer Lambda 35 (the PO samples) and Shimadzu UV-2600 (the SO samples) dual-beam spectrophotometers equipped with integrating spheres. As a reference, a wet filter was used. In order to separate the light absorption of all particles ($a_{\mathrm{p}}(\lambda)$) into $a_{\mathrm{ph}}(\lambda)$ and absorption by non-algal particles ($a_{\mathrm{NAP}}(\lambda)$), the pigments were extracted with hot methanol [29] and hot distilled water [30]. Then OD of the bleached particles on the filter (non-algal particles, NAP) was measured. The OD spectra were adjusted so that the average OD at 715–750 nm was equal to zero. Correction for path-length amplification was applied in accordance with [31]. The $a_p(\lambda)$, m^{-1} and $a_{\mathrm{NAP}}(\lambda)$, m^{-1} were calculated using the equation:

$$a_i(\lambda) = 2.303 \cdot \frac{OD_{\frac{\mathrm{i}}{\mathrm{corr}}}(\lambda)}{(V/S)},$$

where i denotes p or NAP, 2.303 = ln 10, V is the water sample volume, m^3; and S is the filter clearance area, m^2.

The $a_{\mathrm{ph}}(\lambda)$, m^{-1}, was calculated using the equation:

$$a_{\mathrm{ph}}(\lambda) = a_p(\lambda) - a_{\mathrm{NAP}}(\lambda).$$

Chlorophyll a-specific absorption coefficient of phytoplankton ($a^*_{\mathrm{ph}}(\lambda)$, m^2·mg^{-1}) was calculated by dividing $a_{\mathrm{ph}}(\lambda)$, m^{-1} by *TChl-a*, mg·m^{-3}.

The relationship between $a_{\mathrm{ph}}(\lambda)$ and *TChl-a* was described by a power function [32]:

$$a_{\mathrm{ph}}(\lambda) = A(\lambda) \times (TChl\text{-}a)^{B(\lambda)},$$

where $A(\lambda)$ is a spectral coefficient, m^2·mg^{-1}; $B(\lambda)$ is a spectral power coefficient, dimensionless.

Water transparency was assessed based on Secchi disk visibility (Z_{s}, m).

The daily value of photosynthetically available radiation (PAR) incident on the sea surface (PAR(0), E·m^{-2}·d^{-1}) was measured with LI-COR (on the wheelhouse roof) throughout the entire expedition.

Spectral downwelling irradiance ($E_{\mathrm{d}}(\lambda)$, E·m^{-2}·d^{-1}) was measured at each station within the euphotic zone at 1 m intervals using a submersible spectroradiometer RAMSES (TriOS Mess- und Datentechnik GmbH, Germany). The PAR value (E·m^{-2}·day^{-1}) at depth z at the time of sampling was calculated by integrating measured $E_{\mathrm{d}}(\lambda)$ over the visible domain (400–700 nm):

$$PAR(z) = \int_{400}^{700} E_d\,(z,\lambda)\,d\lambda.$$

[2] Neeley, A.R. and Mannino, A., eds., 2018. *Inherent Optical Property Measurements and Protocols: Absorption Coefficient*. IOCCG Ocean Optics and Biogeochemistry Protocols for Satellite Ocean Colour Sensor Validation; vol. 1.0. Dartmouth, NS, Canada: IOCCG, 83 p.

Based on these data, the bottom of the euphotic zone (Z_{eu}) was estimated as the depth at which PAR was 1% of the value just below the sea surface (PAR(0^-)) [33]; the first optical depth for PAR (Z_{1opt}) was estimated as the depth with 37% of PAR(0^-) [34], which is acceptable for relatively homogeneous layers, for example, the upper mixed layer (UML) [35].

The UML depth (Z_{UML}) was assessed using a water density difference criterion (0.2 kg·m^{-3}) from a near-surface (at 1 m) value [36]. The daily PAR averaged over the UML (PAR_{UML}) was calculated using daily PAR(0) measured with LI-COR, in accordance with [37]:

$$PAR_{UML} = 0.94 \cdot PAR(0) \cdot \frac{\left[1 - e^{-4.6\frac{Z_{UML}}{Z_{eu}}}\right]}{4.6\frac{Z_{UML}}{Z_{eu}}},$$

where 0.94 is the coefficient for converting [3] from PAR(0) to PAR(0^-).

Results

The surface temperature of the PO (17–30 August 2023) varied from 9.9 to 16.0 °C and averaged 13.8 ± 1.48 °C (Table 1). Surface salinity varied from 23 to 32 PSU. At most stations, salinity was close to the average value of 30.8 ± 1.48 PSU, and only at shallow-water (22–26 m) stations in Avacha Bay (st. *1–3*) surface salinity was lower (23–27 PSU), which was associated with discharge from the Avacha River.

Table 1

Hydrophysical and bio-optical characteristics of the Pacific Ocean and the Sea of Okhotsk waters in August – September, 2023

Region	Parameter	*t*	*S*	Z_s	Z_{eu}	Z_{1opt}	Z_{UML}	PAR_{UML}	*TChl-a*
PO	*av* ± *SD*	13.8 ± 1.5	30.0 ± 1.5	6.4 ± 2.4	20 ± 6.4	3.1 ± 1.0	3.9 ± 2.4	14.1 ± 6.7	2.8 ± 2.9
	min – max	9.9–16.0	23.0–32.0	2.0–10.0	8.0–35.0	1.2–5.5	2.0–11.0	3.0–27.0	0.67–14
SO	*av* ± *SD*	10.9 ± 1.6	32.3 ± 0.4	7.8 ± 2.0	27 ± 9.8	4.0 ± 1.3	11.2 ± 6.3	7.2 ± 5.8	2.9 ± 1.3
	min – max	7.5–12.9	30.5–32.6	5.0–13.0	14.0–47.0	2.2–7.5	2.0–24.0	0.77–22.0	1.2–5.5

Comments: *t* is surface temperature, °C; *S* is surface salinity, PSU; Z_{1opt} is the first optical depth, m; Z_s is the Secchi disk depth, m; Z_{eu} is the euphotic-zone depth, m; Z_{UML} is the upper mixed-layer depth, m; PAR_{UML} is the average level of photosynthetically available radiation in the UML, E·m^{-2}·d^{-1}; *TChl-a* is the concentration of chlorophyll *a* plus phaeopigments in the surface layer, mg·m^{-3}; *av* is the average value; *SD* is standard deviation.

The surface temperature in the SO during the study period (from 31 August to 9 September 2023) was lower (7.5–12.9 °C with an average of 10.9 ± 1.58 °C) than in the PO. The surface salinity varied in a narrow range (30.5–32.6 PSU), averaging 32.3 ± 0.36 PSU (Table 1). Within the studied water layer, which extended to the bottom at shallow-water stations and to 50 m in other areas, the temperature decreased and the salinity increased with depth. As a result, the waters were density stratified. In the PO, the maximum vertical density gradient ($\Delta\sigma$) varied

[3] Mankovsky, V.I., 1996. [*Fundamentals of Ocean Optics*]. Study Guide. Sevastopol: Marine Hydrophysical Institute, National Academy of Sciences of Ukraine, 119 p. (in Russian).

among stations from 0.19 to 2.5 kg·m^{-4} with a mean of 0.61 ± 0.40 kg·m^{-4}. In the SO, the $\Delta\sigma$ values were lower: from 0.019 to 0.74 kg·m^{-4} with an average value (0.22 ± 0.16 kg·m^{-4}) three times lower than in the PO.

Zs values ranged from 2.0 to 10 m (mean 6.4 ± 2.4 m) in the PO, which was lower than in the SO (range 5.0–13 m; mean 7.8 ± 2.0 m) (Table 1). The least clear waters were observed in Avacha Bay (Fig. 1). The Z_{eu} in the PO was shallower (8.0–35 m, on average 20 ± 6.4 m) compared to the SO (14–47 m, on average 27 ± 9.8 m).

The ranges and mean values of Z_{1opt} and Z_{UML} are given in Table 1. The Z_{1opt} values were mainly (at most stations) within the UML (Fig. 2).

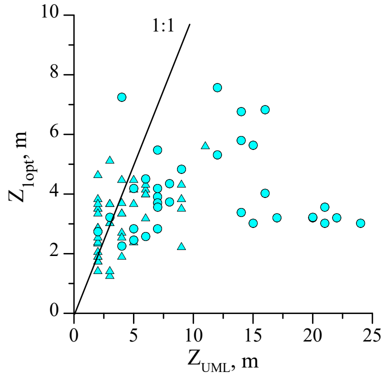

F i g. 2. Relationships between the first optical depth Z_{1opt} and the upper mixed layer depth Z_{UML} in the Pacific Ocean (triangles) and in the Sea of Okhotsk (circles) in August–September 2023

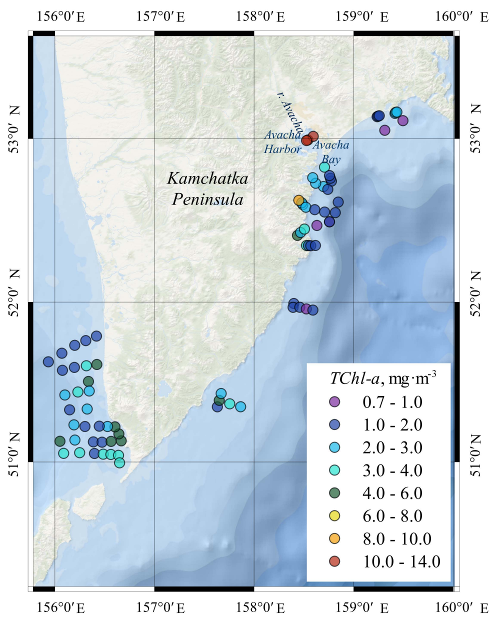

F i g. 3. Surface concentration of chlorophyll *a* plus phaeopigments (*TChl-a*) in the Pacific Ocean (17–30 August 2023) and in the Sea of Okhotsk (31 August–9 September 2023) near the southern part of the Kamchatka Peninsula

In the study area *TChl-a* was highly variable (Table 1, Fig. 3). In the PO *TChl-a* ranged from 0.67 (st. *33*) to 14 mg·m^{-3} (st. *1*) within the layer from the surface to the first optical depth (0–Z_{1opt}) and from 0.67 (st. *33*) to 16 mg·m^{-3} (st. *44*) within the euphotic zone (0–Z_{eu}). In the 0–Z_{1opt} layer relatively high values of *TChl-a* (10–14 mg·m^{-3}) were observed in the desalinated waters in Avacha Bay, low values of *TChl-a* (< 1 mg·m^{-3}) were observed in shelf waters (Figs. 3, 4), which reflects the influence of the river runoff on the *TChl-a*.

In the SO, the *TChl-a* values varied in a narrower range compared with the PO: from 1.2 mg·m^{-3} to 7.7 mg·m^{-3} in the 0–Z_{1opt} layer and from 0.87 mg·m^{-3} to 8.9 mg·m^{-3} in the euphotic zone. The coastal waters (st. *50*, *59*, *60*, *63*, *68*, *70*) were characterised by relatively high *TChl-a* values in the surface layer (> 4 mg·m^{-3}) (Fig. 3). The range of *TChl-a* variability in the 0–Z_{1opt} layer differed between the PO and the SO. However, the mean *TChl-a* values were close: (3.0 ± 3.0) and (3.3 ± 1.6) mg·m^{-3} in the PO and the SO, respectively.

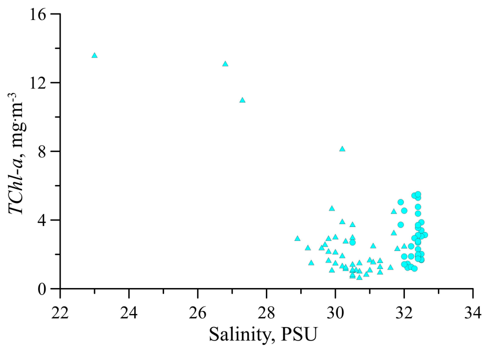

F i g. 4. Relationships between the surface concentration of chlorophyll *a* plus phaeopigments (*TChl-a*) and water salinity in the Pacific Ocean (triangles) and in the Sea of Okhotsk (circles) in August–September 2023

In the study area, waters were stratified and a vertical density gradient **(**$\Delta\sigma_t$**)** occurred within the 0–Z_{eu} layer at almost all stations except for a few stations (st. *77–79*) in the SO (Fig. 1), where Z_{UML} (20–25 m) was close to Z_{eu} (Fig. 5). The density stratification determined the vertical distribution of the *TChl-a* (Fig. 5). Four types of chlorophyll *a* fluorescence profiles can be distinguished based on the position of the fluorescence maximum relative to the surface, the density gradient, and the bottom of the euphotic zone (Fig. 5). These types are characterised by the following features:

1) profiles with a fluorescence maximum in the UML (7–8 m) and a sharp decrease in chlorophyll *a* content in the lower layers. This type was observed in the highly productive waters of Avacha Bay (st. *1–3*);

2) profiles with a narrow and strong fluorescence maximum in the density-gradient layer **(**$\Delta\sigma t$**)** (Fig. 5). In waters with a high-density gradient ($\Delta\sigma_t$ ~ 0.8 kg·m^{-4}), at stations *41–44*, the *TChl-a* values (5.1–16 mg·m^{-3}) at the fluorescence maximum were about an order of magnitude higher than at the surface (1.0–1.7 mg·m^{-3});

3) profiles with a fluorescence maximum below the density-gradient layer ($\Delta\sigma t$), near the bottom of the euphotic zone;

4) profiles with a uniform distribution of *TChl-a* in the euphotic zone, when there is no stratification within the euphotic zone (st. *77–79*).

Chlorophyll *a* fluorescence profiles of the first to third types were observed in both the PO and the SO (Fig. 5), while the fourth type was only seen in the SO at stations with deep mixing. In the PO, stratification within the euphotic zone was noted at all stations. In the SO, it was observed at almost all stations, except for a few (st. *77–79*), where Z_{UML} was close to Z_{eu} and even exceeded it (Fig. 5).

The shape of the spectrum $a_{ph}(\lambda)$ was characterised by the presence of two maxima: in the blue region at a wavelength of 438 nm ($a_{ph}(438)$) and in the red region at a wavelength of 675 nm ($a_{ph}(675)$). At the surface, the $a_{ph}(675)$ and $a_{ph}(438)$ varied within an order of magnitude: from 0.018 to 0.20 m^{-1} and from 0.049 to 0.31 m^{-1}, respectively. In the UML, the $a_{ph}(675)$ and $a_{ph}(438)$ varied in a wider range (from 0.018 to 0.26 and from 0.049 to 0.50 m^{-1}**).** The $a_{ph}(675)$ and $a_{ph}(438)$ variability in the Z_{eu} (from 0.018 to 0.26 m^{-1} and from 0.029 to 0.50 m^{-1}) was close to the one in the UML. Light absorption by phytoplankton is associated with the complex of pigments in the microalgae cells [38]. However, the parameterisation of light absorption by phytoplankton is aimed at obtaining a relationship between $a_{ph}(\lambda)$ and *TChl-a* [32]. This is due to the fact that chlorophyll *a* is the main photosynthetically active pigment, which determines its ecological significance as an indicator of water productivity.

Due to vertical density stratification, two quasi-isolated layers formed within the euphotic zone and differed in their environmental factors, in particular, light intensity (Table 2). Therefore, the link $a_{ph}(\lambda)$ vs *TChl-a* was analysed for the following layers: the UML, the layer between Z_{UML} and the Z_{eu} (depth of 1% PAR) and the layer between Z_{eu} and depth of 0.1% PAR ($Z_{0.1\%}$) (Fig. 6, Table 2).

Coefficients of the relationship $a_{ph}(\lambda)$ (at wavelengths of 438 and 675 nm) vs. *TChl-a* obtained for the UML differed from the coefficients for the layer between UML and Z_{eu} ($p < 0.0001$) and for the layer between Z_{eu} and $Z_{0.1\%}$ ($p < 0.0001$) (Fig. 6). At the same time, no statistically significant differences between the PO and the SO were found within a particular layer ($p < 0.1$). Coefficient $A(\lambda)$ decreased from layer to layer, which was more marked in the blue region: 0.058, 0.043, and 0.034 m²·mg⁻¹ (Table 2).

Type 1

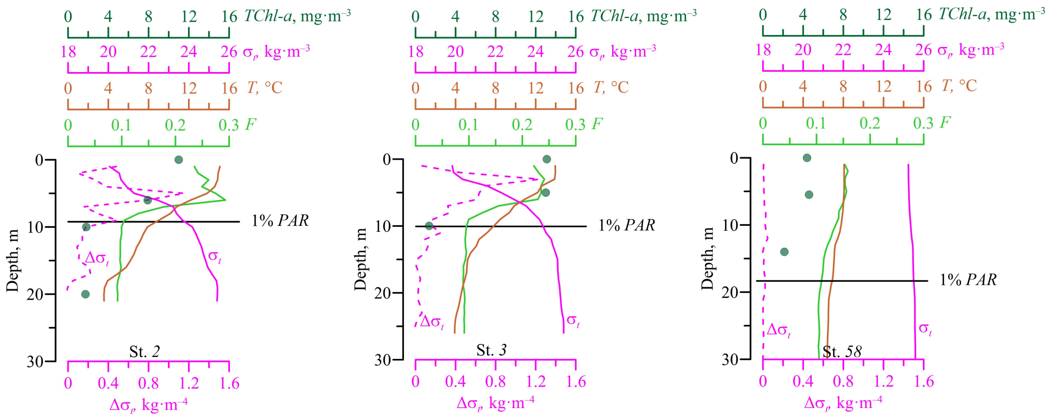

the Pacific Ocean the Sea of Okhotsk

Continuation of Fig. 5

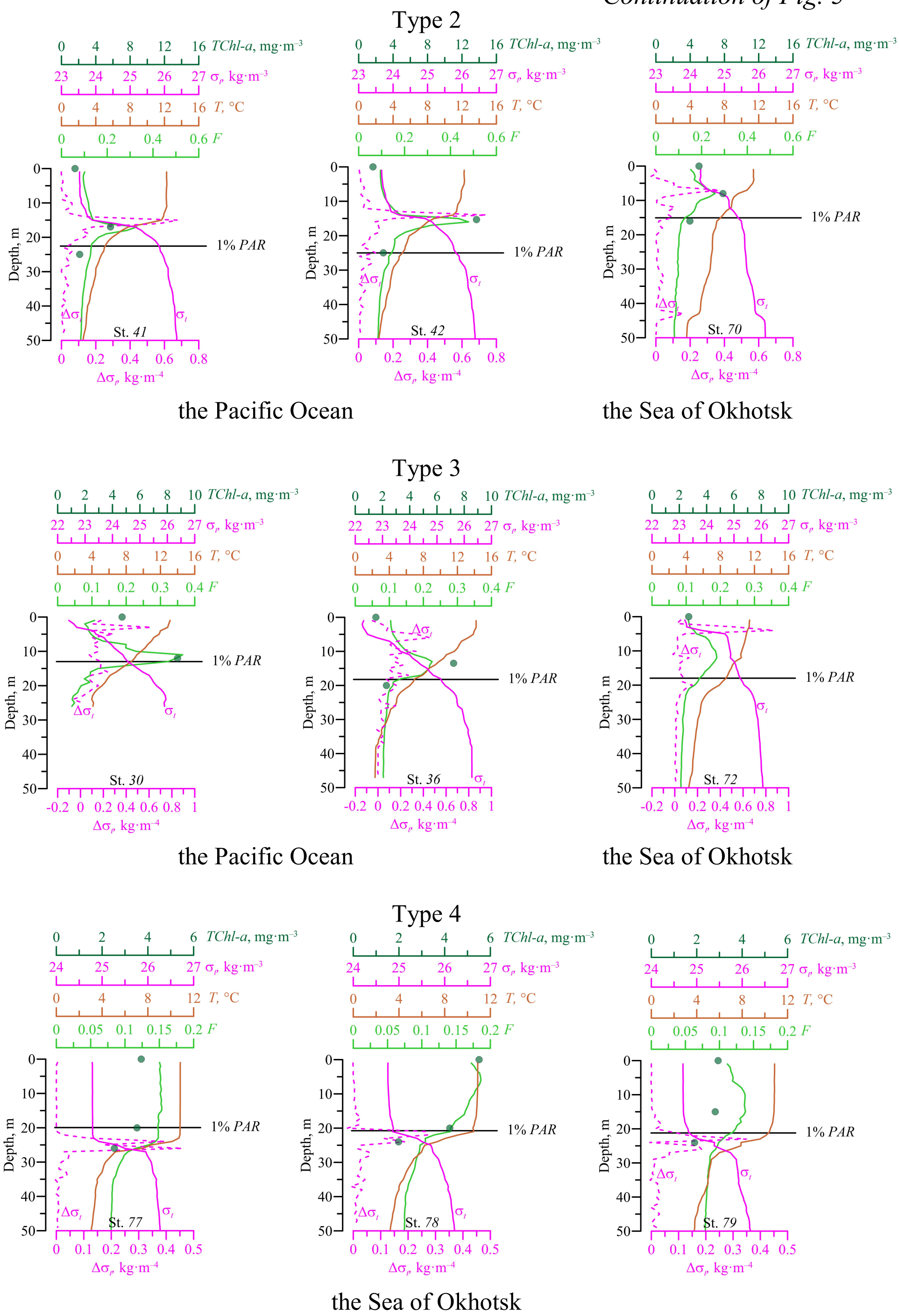

F i g. 5. Types of chlorophyll *a* vertical distribution based on chlorophyll *a* fluorescence (*F*) and concentration of chlorophyll *a* plus phaeopigments measured by a spectrophotometric method (*TChl-a*), water temperature (*T*), water density (σ_t), and vertical gradient of σ_t ($\Delta\sigma_t$) at particular stations in the Pacific Ocean (19–30 August 2023) and in the Sea of Okhotsk (31 August–9 September 2023) off the Kamchatka Peninsula. The black line indicates the euphotic zone (1% PAR)

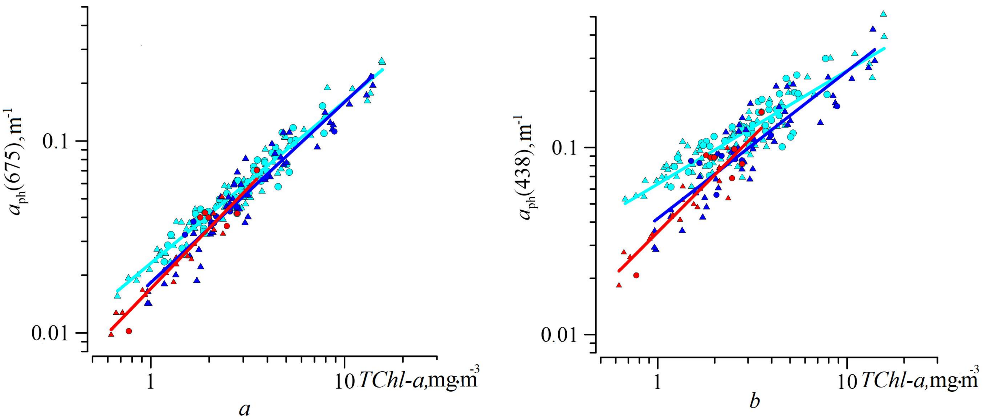

F i g. 6. Power-law dependence of phytoplankton light absorption coefficient at the 675 nm ($a_{ph}(675)$, m^{-1}) (*a*) and 438 nm ($a_{ph}(438)$, m^{-1}) (*b*) wavelengths on the concentration of chlorophyll *a* plus phaeopigments (*TChl-a*) in the Pacific Ocean (triangles) and in the Sea of Okhotsk (circles) for the UML (turquoise colour), the layer between the UML and the bottom of the euphotic zone Z_{eu} (blue colour), and the layer between Z_{eu} and the 0.1% PAR depth (red colour)

T a b l e 2

Coefficients ($A(\lambda)$, m^2·mg^{-1}, and $B(\lambda)$) of the power relationship $a_{ph}(\lambda) = A(\lambda)\ (TChl\text{-}a)^{B(\lambda)}$ for different water layers

Layers	*PAR* ± *SD*	*n*	*A*(438)	*B*(438)	r^2	*A*(675)	*B*(675)	r^2
UML	11.0 ± 7.3	122	0.058	0.606	0.81	0.0231	0.843	0.94
$Z_{UML} - Z_{eu}$	2.3 ± 3.0	60	0.043	0.788	0.81	0.0203	0.94	0.92
$Z_{eu} - Z_{0.1\%}$	0.48 ± 1.30	25	0.0340	1.03	0.78	0.0162	1.03	0.83

Comments: UML is the upper mixed layer; Z_{UML} is the lower boundary of UML; Z_{eu} is the bottom of the euphotic zone; $Z_{0.1\%}$ is the 0.1% photosynthetically available radiation depth; *n* is the number of data points; *PAR* ± *SD* is the mean PAR value for the layer and standard deviation, E·m^{-2}·d^{-1}.

Value of the coefficient $A(\lambda)$ corresponds to $a^*_{ph}(\lambda)$ at *TChl-a* equal to 1 mg m^{-3}. Therefore, the decrease in $A(\lambda)$ reflects the decrease in $a^*_{ph}(\lambda)$ with depth. Comparison of the $a^*_{ph}(\lambda)$ between layers within the euphotic zone (*UML* and layer between Z_{UML} and Z_{eu}) shows that the average $a^*_{ph}(\lambda)$ differed significantly between the layers.

The relationship between $a_{ph}(\lambda)$ (at wavelength of 438 and 675 nm) and *TChl-a* in both layers within the euphotic zone was described by a power function with coefficient $B(\lambda) < 1$ (Table 2), which reflects the decrease in $a^*_{ph}(\lambda)$ with the increase of *TChl-a* (Fig. 6). The coefficient $B(\lambda)$ obtained for the UML was lower than in the deeper layers (Table 2), which indicates a more pronounced decrease in $a^*_{ph}(\lambda)$ with an increasing *TChl-a* in the UML.

The Z_{UML} values varied in a wide range: from 2 to 11 m in the PO and from 2 to 24 m in the SO (Table 1). Due to the high variability of Z_{UML} and Z_s, which determine the light conditions in the UML, the PAR_{UML} values varied within an order of magnitude or more: from 3 to 27 and from 0.77 to 22 E·m^{-2}·d^{-1} in the PO and the

SO, respectively (Table 1). Although the PAR_{UML} varied by an order of magnitude, a weak correlation between the PAR_{UML} and the $a^*_{\mathrm{ph}}(675)$ was observed (Fig. 7). Variability in $a^*_{\mathrm{ph}}(675)$ under similar light conditions in the UML was caused by *TChl-a*. Thus, in the SO under similar PAR_{UML} (12–16 $\mathrm{E \cdot m^{-2} \cdot d^{-1}}$), the values of $a^*_{\mathrm{ph}}(675)$ decreased approximately twofold while *TChl-a* increased approximately fivefold (Fig. 7, points in the ellipse). It should be noted that the decrease in $a^*_{\mathrm{ph}}(675)$ was accompanied by a decrease in R (Fig. 7), which was caused by a more significant decrease in $a^*_{\mathrm{ph}}(\lambda)$ in the blue region, while *TChl-a* increased.

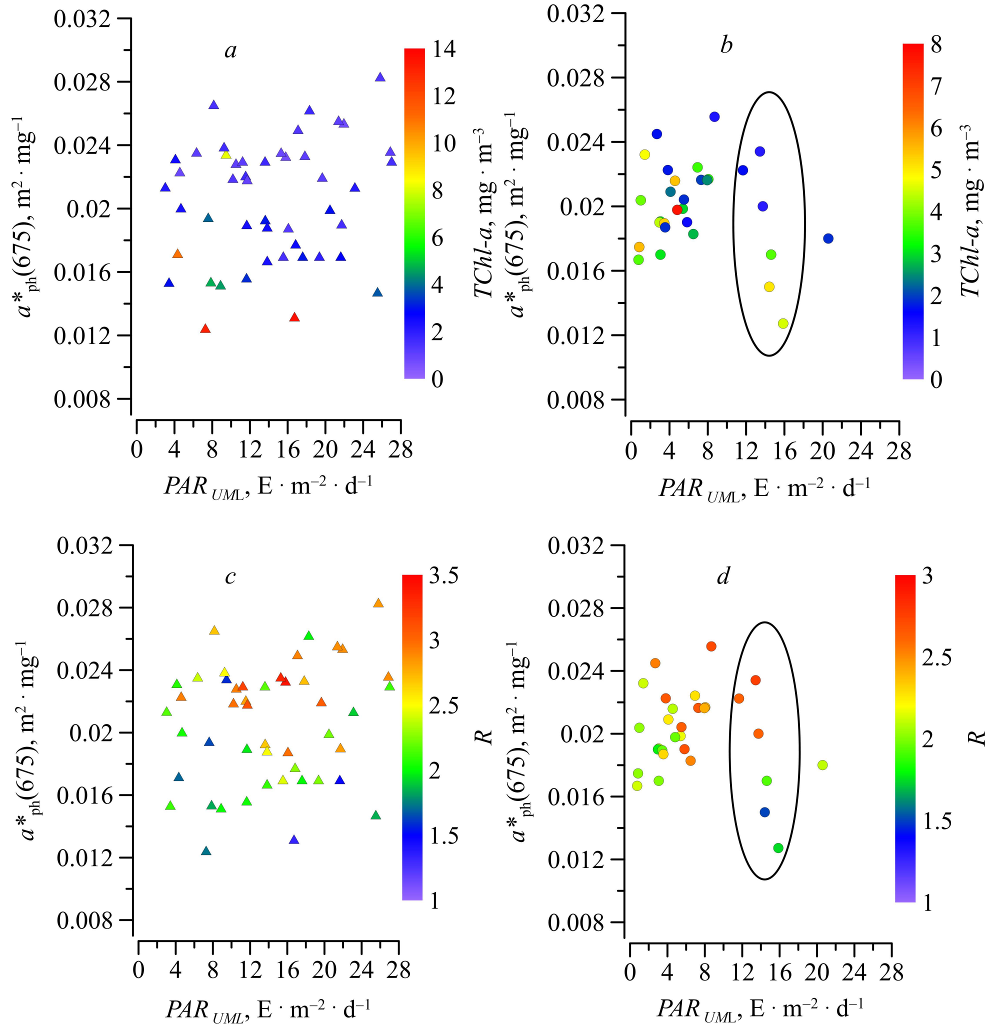

F i g. 7. Relationships between the chlorophyll *a* specific coefficient of phytoplankton light absorption at the 675 nm ($a^*_{\mathrm{ph}}(675)$) wavelength and the average photosynthetically available radiation in the upper mixed layer (PAR_{UML}) in the Pacific Ocean (triangles) (*a*, *c*) and in the Sea of Okhotsk (circles) (*b*, *d*)

To retrieve the $a_{ph}(\lambda)$ spectra based on the *TChl-a* data, the $a_{ph}(\lambda)$ vs. *TChl-a* relationship was parameterised for the layers within the visible domain (400–700 nm) with a spectral resolution of 2 nm (Fig. 8, Supplements 1 and 2).

The $A(\lambda)$ values for the layers within the euphotic zone exceed the $A(\lambda)$ for the oceanic waters [32]. For the layer below Z_{eu}, the $A(\lambda)$ values coincide with those for oceanic waters [32] (Fig. 8).

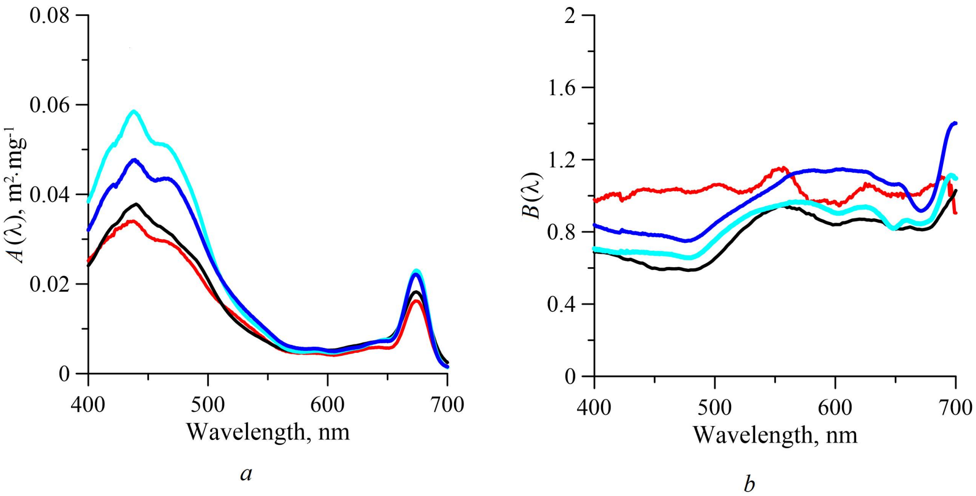

Fig. 8. Spectral coefficients ($A(\lambda)$ (*a*) and $B(\lambda)$ (*b*)) of the dependence of phytoplankton light absorption coefficient ($a_{ph}(\lambda)$) on the concentration of chlorophyll *a* plus phaeopigments (*TChl-a*) – $a_{ph}(\lambda) = A(\lambda) \cdot (TChl\text{-}a)^{B(\lambda)}$ – for the UML (turquoise colour), the layer between UML and the bottom of the euphotic zone Z_{eu} (blue colour), and the layer between Z_{eu} and the 0.1% PAR depth (red colour) in shelf waters near the Kamchatka Peninsula. The black line corresponds to the relationship coefficients obtained for the global ocean [32]

Discussion

The research area was characterised by high variability in the parameters being studied. Values of the *TChl-a* varied by one to two orders of magnitude (0.7 to 14 mg·m^{-3}) at the surface. High *TChl-a* values were observed in coastal desalinated waters (Fig. 3). Relatively high values of the *TChl-a* were noted in the coastal desalinated waters (see Fig. 3), resulting from coastal and river runoff [12–14] that brings the necessary nutrients (P, Si, N and Fe) for phytoplankton growth [39], mainly of volcanic origin [12, 13].

The observed diversity of *TChl-a* vertical profiles (Fig. 5) is the result of the interaction of a complex of factors: nutrient supply and hydrophysical characteristics such as light intensity, vertical density stratification and water mixing [33, 40, 41]. A change in a key factor leads to the formation of a certain type of *TChl-a* vertical profile [42].

During vertical water stratification within the euphotic zone, the *TChl-a* profile is characterised by the presence of a maximum, the position of which depends on environmental factors. The *TChl-a* profile with a deep chlorophyll *a* maximum near the Z_{eu} (DCM) (type 3, Fig. 5) occurs because active phytoplankton growth in the UML leads to nutrient depletion there [33, 43]. Relatively high values of the *TChl-a* in the DCM are caused mainly by an adaptive increase in intracellular chlorophyll *a* content and only partially by an increase in phytoplankton abundance [42, 43]. The formation of the profile with a subsurface maximum of *TChl-a* (type 1, Fig. 5) is related to a permanent nutrient supply in the subsurface layer (desalination of Avacha Bay can be considered as a marker of the permanent nutrient supply) [33, 42]. In the stratified waters another profile was identified. This profile has the *TChl-a* maximum within the density-gradient layer (type 2, Fig. 5), which is related to favourable conditions (light intensity and nutrient availability) for phytoplankton growth [40, 41].

In the absence of stratification within the euphotic zone, a uniform distribution of *TChl-a* (type 4, Fig. 5) is observed due to active vertical mixing [33, 43].

Values of the $a_{ph}(\lambda)$ and *TChl-a* varied in a wide range, which made it possible to reveal relationships between these parameters for the visible range of light with an interval of 2 nm for two layers of the euphotic zone and the underlying layer (Supplements 1 and 2) (Fig. 8). The results of the parameterisation make it possible to retrieve the $a_{ph}(\lambda)$ spectra from *TChl-a*, which is needed for modelling the spectral downwelling irradiance in the sea and calculating the primary production of phytoplankton. Z_{1opt} was located within the UML at most stations (Fig. 2), and consequently bio-optical properties of the UML determine spectral water-leaving radiance [44]. Therefore, coefficients of the $a_{ph}(\lambda)$ vs. *TChl-a* relationship obtained for the UML (Supplements 1 and 2) can be used to develop a regional satellite algorithm, in particular to assess *TChl-a* based on $a_{ph}(\lambda)$ retrieved using satellite data and algorithms like the three-band algorithm [24]. The application of the regional parameterisation provides a more accurate retrieval of *TChl-a* values compared to the standard products, which overestimated *TChl-a* by up to 260% in the SO [19, 45].

The decrease in $a^*_{ph}(\lambda)$ with an increase in *TChl-a* (see Fig. 7) was probably due to an increase in the proportion of large-celled species in the phytoplankton. Studies in waters with different trophic status (from hyper-oligotrophic to eutrophic) showed that an increase in *TChl-a* was accompanied by an increase in mean cell size of phytoplankton [46–49]. The twofold decrease observed in our study in $a^*_{ph}(678)$ (from 0.025 to 0.012 $m^2 \cdot mg^{-1}$) under similar PAR_{UML} and an increase in *TChl-a* (Fig. 7) was probably related to an increase in average cell size of phytoplankton from ~ 5 to ~ 20 µm [50, 51]. The decrease in $a^*_{ph}(675)$ and *R* as the size of microalgal cells increases [46, 52] is due to an increase in the degree of self-shading of pigments within the cells [53].

The revealed difference between the layers of the euphotic zone in the $A(\lambda)$ and $B(\lambda)$ coefficients in the relationship $a_{ph}(\lambda)$ vs. *TChl-a* (see Fig. 8, Table 2) was due to a decrease in $a^*_{ph}(\lambda)$ (under similar *TChl-a*) with depth from one layer to another, resulting from changes in the intracellular pigment concentration, content of accessory pigments (relative to *TChl-a*) [32, 54–57] and species and size structure of phytoplankton [56–59] during adaptation to environmental factors (light, temperature and nutrients) [60–62]. The greatest degree of variability in intracellular pigment concentration is caused by the influence of light [61]. A comparison of the parameterisation of phytoplankton absorption (the coefficients $A(438)$ and $A(675)$) among different seasons and regions showed a relationship with the light conditions ($r^2 = 0.99$ and $r^2 = 0.94$) (Fig. 9). Values of $A(438)$ and $A(675)$ were almost the same in different regions (the UML of the Black Sea in winter and the layer between Z_{UML} and Z_{eu} in the study area) under similar PAR_{UML}. This means that differences in phytoplankton absorption parameterisation between layers of the euphotic zone and between regions were associated with adaptive changes at the cellular level (the intracellular pigment concentration) and at the community level (the species/size structure of phytoplankton) mainly under the influence of light.

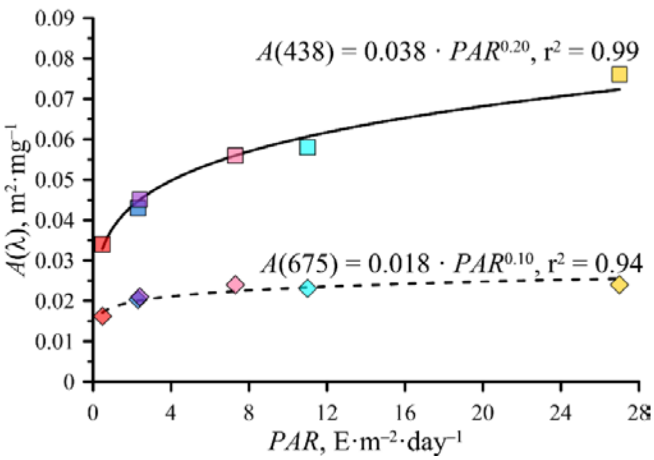

F i g. 9. Impact of photosynthetically available radiation (PAR) on coefficient $A(\lambda)$ in equation $a_{ph}(\lambda)=A(\lambda)\cdot TChl\text{-}a^{B(\lambda)}$ in the study area for the UML (turquoise), for the layer between the UML and optical depth 4.6 (blue), and for the layer between optical depths 4.6 and 6.9 (red); in the UML of the Black Sea (summer in yellow and winter in purple) [56]; in the UML of the Barents Sea, the Norwegian Sea and the adjacent Arctic Ocean (pink) [63]. Values of $A(438)$ (square) and $A(675)$ (rhombus) are shown

Conclusions

For the first time in the shelf waters of the SO and the PO near the southern part of the Kamchatka Peninsula, the variability of spectral phytoplankton light absorption coefficient and its relationship with the chlorophyll *a* concentration were studied. The study area was characterised by high variability in these parameters (by an order of magnitude or more). The influence of coastal and river runoff on the spatial distribution of these parameters was shown. Four types of vertical distribution of chlorophyll *a* concentration were identified depending on environmental factors. A dependence of chlorophyll *a*-specific absorption coefficient on the PAR and chlorophyll *a* concentration was found, which was due to photoadaptive changes in the intracellular pigment concentration and an increase in the degree of their packaging in large-celled phytoplankton, the proportion of which in the total phytoplankton biomass increases with increasing water trophicity.

For the first time for the study area, parameterisation of phytoplankton light absorption was performed in the wavelength range 400–700 nm (with 2 nm resolution) for two layers within the euphotic zone isolated by density stratification and the underlying layer. Differences between the parameterisation coefficients for the layers were revealed. The obtained coefficients of the $a_{\text{ph}}(\lambda)$ vs *TChl-a* relationship enable correct retrieval of $a_{\text{ph}}(\lambda)$ based on *TChl-a* within the euphotic zone, which is crucial for modelling spectral downwelling irradiance and calculation of primary production as well as for developing a regional satellite algorithm to assess chlorophyll *a* concentration. The obtained results can be used to establish a system of operational monitoring of water productivity and quality indicators off the Kamchatka Peninsula.

REFERENCES

1. Saitoh, S.-I., Kishino, M., Kiyofuji, H., Taguchi, S. and Takahashi, M., 1996. Seasonal Variability of Phytoplankton Pigment Concentration in the Okhotsk Sea. *Journal of the Remote Sensing Society of Japan*, 16(2), pp. 172-178. https://doi.org/10.11440/rssj1981.16.172
2. Sorokin, Yu.I. and Sorokin, P.Yu., 1999. Production in the Sea of Okhotsk. *Journal of Plankton Research*, 21(2), pp. 201-230. https://doi.org/10.1093/plankt/21.2.201
3. Shiomoto, A., Hashimoto, S. and Murakami, T., 1998. Primary Productivity and Solar Radiation off Sanriku in May 1997. *Journal of Oceanography*, 54(5), pp. 539-544. https://doi.org/10.1007/BF02742455
4. Oida, J., Hirawake, T., Yamashita, Y., Abe, H., Nishioka, J., Waga, H., Nomura, D. and Kakehi, S., 2024. Classification of Optical Water Groups in the Subarctic Pacific and Adjacent Seas Using Satellite-Derived Light Absorption Spectra of Chromophoric Dissolved Organic Matter. *Deep-Sea Research Part I: Oceanographic Research Papers*, 208, 104313. https://doi.org/10.1016/j.dsr.2024.104313
5. Mundo, R., Matsunaka, T., Nakanowatari, T., Taniuchi, Y., Inoue, M., Kasai, H., Mashita, K., Mitsunushi, H. and Nagao, S., 2024. A Review of the Oceanographic Structure and Biological Productivity in the Southern Okhotsk Sea. *Progress in Oceanography*, 221, 103194. https://doi.org/10.1016/j.pocean.2023.103194
6. Nishioka, J., Mitsudera, H., Yasuda, I., Liu, Y., Nakatsuka, T. and Volkov, Y.N., 2014. Biogeochemical and Physical Processes in the Sea of Okhotsk and the Linkage to the Pacific Ocean. *Progress in Oceanography*, 126, pp. 1-7. https://doi.org/10.1016/j.pocean.2014.04.027
7. Arzhanova, N.V., Naletova, I.A., Sapoznikov, V.V. and Polyakova, A.V., 2002. Phytoplankton Provision with Nutrients in the Northern Part of the Sea of Okhotsk. *Oceanology*, 42(2), pp. 185-196.
8. Kasai, H., Nakano, Y., Ono, T. and Tsuda, A., 2010. Seasonal Change of Oceanographic Conditions and Chlorophyll *a* Vertical Distribution in the Southwestern Okhotsk Sea during the Non-Iced Season. *Journal of Oceanography*, 66, pp. 13-26. https://doi.org/10.1007/s10872-010-0002-3

9. Agatova, A.I., Lapina, N.M. and Torgunova, N.I., 2016. Organic Matter, Its Transformation Rates and the Productivity of Different Regions in the Sea of Okhotsk. *Trudy VNIRO*, 164, pp. 41-61 (in Russian).

10. Waga, H., Fujiwara, A., Hirawake, T., Suzuki, K., Yoshida, K., Abe, H. and Nomura, D., 2022. Primary Productivity and Phytoplankton Community Structure in Surface Waters of the Western Subarctic Pacific and the Bering Sea during Summer with Reference to Bloom Stages. *Progress in Oceanography*, 201, 102738. https://doi.org/10.1016/j.pocean.2021.102738

11. Tskhay, Zh.R. and Shevchenko, G.V., 2022. Distribution Features of Chlorophyll *a* Concentration off the East Coast of Kamchatka in Autumn 2020 from Satellite Data. *Sovremennye problemy distantsionnogo zondirovaniya Zemli iz kosmosa*, 19(1), pp. 226-238 (in Russian). https://doi.org/10.21046/2070-7401-2022-19-1-226-238

12. Semkin, P., Pavlova, G., Lobanov, V., Barabanshchikov, Y., Kukla, S., Sagalaev, S., Shvetsova, M., Shkirnikova, E., Tishchenko, P. [et al.], 2023. Nutrient Flux under the Influence of Melt Water Runoff from Volcanic Territories and Ecosystem Response of Vilyuchinskaya and Avachinskaya Bays in Southeastern Kamchatka. *Journal of Marine Science and Engineering*, 11(7), 1299. https://doi.org/10.3390/jmse11071299

13. Semkin, P., Pavlova, G., Lobanov, V., Baigubekov, K., Barabanshchikov, Y., Gorin, S., Shvetsova, M., Shkirnikova, E., Ulanova, O. [et al.], 2025. Nutrient Fluxes from the Kamchatka and Penzhina Rivers and Their Impact on Coastal Ecosystems on Both Sides of the Kamchatka Peninsula. *Journal of Marine Science and Engineering*, 13(3), 569. https://doi.org/10.3390/jmse13030569

14. Lobanov, V.B., Sergeev, A.F., Semkin, P.Y., Lukyanova, N.B., Tsoy, V., Tishchenko, P.P., Alekseev, I.F., Kukla, S.P., Mazur, A.A. [et al.], 2023. Study of Abiotic Factors Controlling Marine Ecosystem Dynamics and Formation of Anomalous Conditions in Coastal Waters of the Far East in the 80th Cruise of the R/V Professor Gagarinskiy. *Oceanology*, 63(6), pp. 931-933. https://doi.org/10.1134/S0001437023060085

15. Bondur, V., Zamshin, V., Chvertkova, O., Matrosova, E. and Khodaeva, V., 2021. Detection and Analysis of the Causes of Intensive Harmful Algal Bloom in Kamchatka Based on Satellite Data. *Journal of Marine Science and Engineering*, 9(10), 1092. https://doi.org/10.3390/jmse9101092

16. Orlova, T.Y., Konovalova, G.V., Stonik, I.V., Selina, M.S., Morozova, T.V. and Shevchenko, O.G., 2002. Harmful Algal Blooms on the Eastern Coast of Russia. In: F.J.R. Taylor and V.L. Trainer, eds., 2002. *Harmful Algal Blooms in the PICES Region of the North Pacific.* PICES Scientific Report No. 23. Sidney, BC: North Pacific Marine Science Organization (PICES), pp. 47-73.

17. Orlova, T.Y., Aleksanin, A.I., Lepskaya, E.V., Efimova, K.V., Selina, M.S., Morozova, T.V., Stonik, I.V., Kachur, V.A., Karpenko, A.A. [et al.], 2022. A Massive Bloom of Karenia Species (Dinophyceae) off the Kamchatka Coast, Russia, in the Fall of 2020. *Harmful Algae*, 120, 102337. https://doi.org/10.1016/j.hal.2022.102337

18. Adjovu, G.E., Stephen, H., James, D. and Ahmad, S., 2023. Overview of the Application of Remote Sensing in Effective Monitoring of Water Quality Parameters. *Remote Sensing*, 15(7), 1938. https://doi.org/10.3390/rs15071938

19. Takao, S., Iida, T., Isada, T., Saitoh, S.-I., Hirata, T. and Suzuki, K., 2014. Bio-Optical Properties during the Summer Season in the Sea of Okhotsk. *Progress in Oceanography*, 126, pp. 233-241. https://doi.org/10.1016/j.pocean.2014.04.010

20. Zakharkov, S.P., Lepskaya, E.V., Tepnin, O.B., Shtraikhert, E.A. and Gordeichuk, T.N., 2020. Primary Production of the Avacha Bay in Summer 2017. *Vestnik of the Far East Branch of the RAS*, (1), pp. 83-89. https://doi.org/10.25808/08697698.2020.209.1.009 (in Russian)

21. Mobley, C.D., Stramski, D., Bissett, W.P. and Boss, E., 2004. Optical Modeling of Ocean Waters: Is the Case 1 – Case 2 Classification Still Useful? *Oceanography*, 17(2), pp. 60-67. https://doi.org/10.5670/oceanog.2004.48

22. Schofield, O., Arnone, R.A., Bissett, W.P., Dickey, T.D., Davis, C.O., Finkel, Z., Oliver, M. and Moline, M.A., 2004. Watercolors in the Coastal Zone: What Can We See? *Oceanography*, 17(2), pp. 24-31. https://doi.org/10.5670/oceanog.2004.44

23. Saba, V.S., Friedrichs, M.A.M., Carr, M.-E., Antoine, D., Armstrong, R.A., Asanuma, I., Aumont, O., Bates, N.R., Behrenfeld, M.J. [et al.], 2010. Challenges of Modeling Depth-Integrated Marine Primary Productivity over Multiple Decades: A Case Study at BATS and HOT. *Global Biogeochemical Cycles*, 24(3), GB3020. https://doi.org/10.1029/2009GB003655

24. Suslin, V. and Churilova, T.Ya., 2016. A Regional Algorithm for Separating Light Absorption by Chlorophyll-*a* and Coloured Detrital Matter in the Black Sea, Using 480–560 nm Bands from Ocean Colour Scanners. *International Journal of Remote Sensing*, 37(18), pp. 4380-4400. https://doi.org/10.1080/01431161.2016.1211350

25. Jeffrey, S.W. and Humphrey, G.F., 1975. New Spectrophotometric Equations for Determining Chlorophylls a, b, c_1 and c_2 in Higher Plants, Algae and Natural Phytoplankton. *Biochemie und Physiologie der Pflanzen*, 167(2), pp. 191-194. https://doi.org/10.1016/S0015-3796(17)30778-3

26. Lorenzen, C.J., 1967. Determination of Chlorophyll and Pheo-Pigments: Spectrophotometric Equations. *Limnology and Oceanography*, 12(2), pp. 343-346. https://doi.org/10.4319/lo.1967.12.2.0343

27. Yentsch, C.S., 1962. Measurement of Visible Light Absorption by Particulate Matter in the Ocean. *Limnology and Oceanography*, 7(2), pp. 207-217. https://doi.org/10.4319/lo.1962.7.2.0207

28. Mitchell, B.G., 1990. Algorithms for Determining the Absorption Coefficient for Aquatic Particulates Using the Quantitative Filter Technique. In: SPIE, 1990. *Proceedings of SPIE*. Bellingham, WA: SPIE. Vol. 1302: Ocean Optics X, pp. 137-148. https://doi.org/10.1117/12.21440

29. Kishino, M., Takahashi, M., Okami, N. and Ichimura, S., 1985. Estimation of the Spectral Absorption Coefficients of Phytoplankton in the Sea. *Bulletin of Marine Science*, 37(2), pp. 634-642.

30. Roesler, C.S. and Perry, M.J., 1995. In Situ Phytoplankton Absorption, Fluorescence Emission, and Particulate Backscattering Spectra Determined from Reflectance. *Journal of Geophysical Research: Oceans*, 100(C7), pp. 13279-13294. https://doi.org/10.1029/95JC00455

31. Stramski, D., Reynolds, R.A., Kaczmarek, S., Uitz, J. and Zheng, G., 2015. Correction of Pathlength Amplification in the Filter-Pad Technique for Measurements of Particulate Absorption Coefficient in the Visible Spectral Region. *Applied Optics*, 54(22), pp. 6763-6782. https://doi.org/10.1364/AO.54.006763

32. Bricaud, A., Babin, M., Morel, A. and Claustre, H., 1995. Variability in the Chlorophyll-Specific Absorption Coefficients of Natural Phytoplankton: Analysis and Parameterization. *Journal of Geophysical Research: Oceans*, 100(C7), pp. 13321-13332. https://doi.org/10.1029/95JC00463

33. Morel, A. and Berthon, J.-F., 1989. Surface Pigments, Algal Biomass Profiles, and Potential Production of the Euphotic Layer: Relationships Reinvestigated in View of Remote-Sensing Applications. *Limnology and Oceanography*, 34(8), pp. 1545-1562. https://doi.org/10.4319/lo.1989.34.8.1545

34. Kirk, J.T.O., 2010. *Light and Photosynthesis in Aquatic Ecosystems.* 3rd ed. Cambridge: Cambridge University Press, 649 p. https://doi.org/10.1017/CBO9781139168212

35. Mobley, C.D., ed., 2022. *The Oceanic Optics Book*. Dartmouth, NS, Canada: International Ocean Colour Coordinating Group (IOCCG), 924 p. https://doi.org/10.25607/OBP-1710

36. Brainerd, K.E. and Gregg, M.C., 1995. Surface Mixed and Mixing Layer Depths. *Deep Sea Research Part I: Oceanographic Research Papers*, 42(9), pp. 1521-1543. https://doi.org/10.1016/0967-0637(95)00068-H

37. Babin, M., Morel, A., Claustre, H., Bricaud, A., Kolber, Z. and Falkowski, P.G., 1996. Nitrogen- and Irradiance-Dependent Variations of the Maximum Quantum Yield of Carbon Fixation in Eutrophic, Mesotrophic and Oligotrophic Marine Systems. *Deep-Sea Research Part I: Oceanographic Research Papers*, 43(8), pp. 1241-1272. https://doi.org/10.1016/0967-0637(96)00058-1

38. Jeffrey, S.W., Mantoura, R.F.C. and Wright, S.W., eds., 1997. *Phytoplankton Pigments in Oceanography: Guidelines to Modern Methods*. Paris: UNESCO Publishing, 661 p.

39. Duggen, S., Olgun, N., Croot, P., Hoffmann, L., Dietze, H., Delmelle, P. and Teschner, C., 2010. The Role of Airborne Volcanic Ash for the Surface Ocean Biogeochemical Iron-Cycle: A Review. *Biogeosciences*, 7(3), pp. 827-844. https://doi.org/10.5194/bg-7-827-2010

40. Sharples, J., Moore, C.M., Rippeth, T.P., Holligan, P.M., Hydes, D.J., Fisher, N.R. and Simpson, J.H., 2001. Phytoplankton Distribution and Survival in the Thermocline. *Limnology and Oceanography*, 46(3), pp. 486-496. https://doi.org/10.4319/lo.2001.46.3.0486

41. Hickman, A.E., Holligan, P.M., Moore, C.M., Sharples, J., Krivtsov, V. and Palmer, M.R., 2009. Distribution and Chromatic Adaptation of Phytoplankton within a Shelf Sea Thermocline. *Limnology and Oceanography*, 54(2), pp. 525-536. https://doi.org/10.4319/lo.2009.54.2.0525

42. Cullen, J.J., 1982. The Deep Chlorophyll Maximum: Comparing Vertical Profiles of Chlorophyll *a*. *Canadian Journal of Fisheries and Aquatic Sciences*, 39(5), pp. 791-803. https://doi.org/10.1139/f82-108

43. Finenko, Z.Z., Churilova, T.Ya. and Lee, R.I., 2005. Dynamics of the Vertical Distributions of Chlorophyll and Phytoplankton Biomass in the Black Sea. *Oceanology*, 45(1), pp. 112-126.

44. Loisel, H. and Stramski, D., 2000. Estimation of the Inherent Optical Properties of Natural Waters from the Irradiance Attenuation Coefficient and Reflectance in the Presence of Raman Scattering. *Applied Optics*, 39(18), pp. 3001-3011. https://doi.org/10.1364/AO.39.003001

45. Permyakov, M.S., Bukin, O.A., Akmaikin, D.A., Salyuk, P.A. and Podoprigora, E.L., 2004. Regional Algorithms for Retrieving Chlorophyll *a* Concentration Based on SeaWiFS Scanner Data for the Sea of Okhotsk. *Researched in Russia*, 7, pp. 972-981 (in Russian).

46. Ciotti, Á.M., Lewis, M.R. and Cullen, J.J., 2002. Assessment of the Relationships between Dominant Cell Size in Natural Phytoplankton Communities and the Spectral Shape

of the Absorption Coefficient. *Limnology and Oceanography*, 47(2), pp. 404-417. https://doi.org/10.4319/lo.2002.47.2.0404

47. Ras, J., Claustre, H. and Uitz, J., 2008. Spatial Variability of Phytoplankton Pigment Distributions in the Subtropical South Pacific Ocean: Comparison between In Situ and Predicted Data. *Biogeosciences*, 5(2), pp. 353-369. https://doi.org/10.5194/bg-5-353-2008

48. Bricaud, A., Babin, M., Claustre, H., Ras, J. and Tièche, F., 2010. Light Absorption Properties and Absorption Budget of Southeast Pacific Waters. *Journal of Geophysical Research: Oceans*, 115(C8), C08009. https://doi.org/10.1029/2009JC005517

49. Chen, B. and Liu, H., 2010. Relationships between Phytoplankton Growth and Cell Size in Surface Oceans: Interactive Effects of Temperature, Nutrients, and Grazing. *Limnology and Oceanography*, 55(3), pp. 965-972. https://doi.org/10.4319/lo.2010.55.3.0965

50. Roy, S., Sathyendranath, S. and Platt, T., 2011. Retrieval of Phytoplankton Size from Bio-Optical Measurements: Theory and Application. *Journal of the Royal Society Interface*, 8(58), pp. 650-660. https://doi.org/10.1098/rsif.2010.0503

51. Roy, S., Sathyendranath, S., Bouman, H. and Platt, T., 2013. The Global Distribution of Phytoplankton Size Spectrum and Size Classes from Their Light-Absorption Spectra Derived from Satellite Data. *Remote Sensing of Environment*, 139, pp. 185-197. https://doi.org/10.1016/j.rse.2013.08.004

52. Ciotti, Á.M., Cullen, J.J. and Lewis, M.R., 1999. A Semi-Analytical Model of the Influence of Phytoplankton Community Structure on the Relationship between Light Attenuation and Ocean Color. *Journal of Geophysical Research: Oceans*, 104(C1), pp. 1559-1578. https://doi.org/10.1029/1998JC900021

53. Morel, A. and Bricaud, A., 1981. Theoretical Results Concerning Light Absorption in a Discrete Medium, and Application to Specific Absorption of Phytoplankton. *Deep Sea Research Part A. Oceanographic Research Papers*, 28(11), pp. 1375-1393. https://doi.org/10.1016/0198-0149(81)90039-X

54. Bidigare, R.R., Ondrusek, M.E., Morrow, J.H. and Kiefer, D.A., 1990. In-vivo Absorption Properties of Algal Pigments. In: SPIE, 1990. *Proceedings of SPIE*. Bellingham, WA: SPIE. Vol. 1302: Ocean Optics X, pp. 290-302. https://doi.org/10.1117/12.21451

55. Bricaud, A., Claustre, H., Ras, J. and Oubelkheir, K., 2004. Natural Variability of Phytoplanktonic Absorption in Oceanic Waters: Influence of the Size Structure of Algal Populations. *Journal of Geophysical Research: Oceans*, 109(C11), C11010. https://doi.org/10.1029/2004JC002419

56. Churilova, T., Suslin, V., Krivenko, O., Efimova, T., Moiseeva, N., Mukhanov, V. and Smirnova, L., 2017. Light Absorption by Phytoplankton in the Upper Mixed Layer of the Black Sea: Seasonality and Parametrization. *Frontiers in Marine Science*, 4, 90. https://doi.org/10.3389/fmars.2017.00090

57. Churilova, T., Suslin, V., Sosik, H.M., Efimova, T., Moiseeva, N., Moncheva, S., Mukhanov, V., Rylkova, O. and Krivenko, O., 2019. Phytoplankton Light Absorption in the Deep Chlorophyll Maximum Layer of the Black Sea. *European Journal of Remote Sensing*, 52(1), pp. 123-136. https://doi.org/10.1080/22797254.2018.1533389

58. Sosik, H.M. and Mitchell, B.G., 1995. Light Absorption by Phytoplankton, Photosynthetic Pigments and Detritus in the California Current System. *Deep-Sea Research Part I: Oceanographic Research Papers*, 42(10), pp. 1717-1748. https://doi.org/10.1016/0967-0637(95)00081-G

59. Allali, K., Bricaud, A. and Claustre, H., 1997. Spatial Variations in the Chlorophyll-Specific Absorption Coefficients of Phytoplankton and Photosynthetically Active Pigments in the Equatorial Pacific. *Journal of Geophysical Research: Oceans*, 102(C6), pp. 12413-12423. https://doi.org/10.1029/97JC00380

60. Geider, R.J., MacIntyre, H.L. and Kana, T.M., 1997. Dynamic Model of Phytoplankton Growth and Acclimation: Responses of the Balanced Growth Rate and the Chlorophyll *a*: Carbon Ratio to Light, Nutrient Limitation and Temperature. *Marine Ecology Progress Series*, 148, pp. 187-200. https://doi.org/10.3354/meps148187

61. MacIntyre, H.L., Kana, T.M., Anning, T. and Geider, R.J., 2002. Photoacclimation of Photosynthesis Irradiance Response Curves and Photosynthetic Pigments in Microalgae and Cyanobacteria. *Journal of Phycology*, 38(1), pp. 17-38. https://doi.org/10.1046/j.1529-8817.2002.00094.x

62. Flynn, K.J., 2003. Do We Need Complex Mechanistic Photoacclimation Models for Phytoplankton? *Limnology and Oceanography*, 48(6), pp. 2243-2249. https://doi.org/10.4319/lo.2003.48.6.2243

63. Efimova, T., Churilova, T., Skorokhod, E., Suslin, V., Buchelnikov, A.S., Glukhovets, D., Khrapko, A. and Moiseeva, N., 2023. Light Absorption by Optically Active Components in the Arctic Region (August 2020) and the Possibility of Application to Satellite Products for Water Quality Assessment. *Remote Sensing*, 15(17), 4346. https://doi.org/10.3390/rs15174346

Submitted 27.03.2026; approved after review 21.04.2026;
accepted for publication 20.05.2026.

About the authors:

Tatyana Ya. Churilova, Leading Researcher, A.O. Kovalevsky Institute of Biology of the Southern Seas, Russian Academy of Sciences (2 Nakhimov Ave., Sevastopol, 299011, Russian Federation); Leading Researcher, Institute of the World Ocean (School), Far Eastern Federal University (10 Ajax Bay, Russky Island, Vladivostok, 690922, Russian Federation), CSc. (Biol.), **SPIN-code: 2238-9533**, **ORCID ID: 0000-0002-0455-7284**, **Scopus Author ID: 6603622802**, **ResearcherID: O-8437-2016**, tanya.churilova@ibss-ras.ru

Elena Yu. Skorokhod, Researcher, A.O. Kovalevsky Institute of Biology of the Southern Seas, Russian Academy of Sciences (2 Nakhimov Ave., Sevastopol, 299011, Russian Federation); Junior Researcher, Institute of the World Ocean (School), Far Eastern Federal University (10 Ajax Bay, Russky Island, Vladivostok, 690922, Russian Federation) **SPIN-code: 3314-5775**, **ORCID ID: 0000-0002-3057-3964**, **Scopus Author ID: 57215009764**, **ResearcherID: A-6831-2019**, elenaskorokhod@ibss-ras.ru

Natalia A. Moiseeva, Researcher, A.O. Kovalevsky Institute of Biology of the Southern Seas, Russian Academy of Sciences (2 Nakhimov Ave., Sevastopol, 299011, Russian Federation) **SPIN-code: 8946-3315**, **ORCID ID: 0000-0003-1356-7981**, **Scopus Author ID: 57194431032**, **ResearcherID: AAN-2819-2019**, moiseeva@ibss-ras.ru

Anatoly S. Buchelnikov, Leading Researcher, A.O. Kovalevsky Institute of Biology of the Southern Seas, Russian Academy of Sciences (2 Nakhimov Ave., Sevastopol, 299011, Russian Federation); Associate Professor, Sevastopol State University (33 Universitetskaya Str., Sevastopol, 299053, Russian Federation), CSc.(Phys.-Math.), **SPIN-code: 4364-8832**, **ORCID ID: 0000-0002-1853-4671**, **Scopus Author ID: 38661041800**, **ResearcherID: B-2280-2013**, buchelnikov@ibss-ras.ru

Tatyana V. Efimova, Senior Researcher, A.O. Kovalevsky Institute of Biology of the Southern Seas, Russian Academy of Sciences (2 Nakhimov Ave., Sevastopol, 299011, Russian Federation); Senior Researcher, Institute of the World Ocean (School), Far Eastern Federal University (10 Ajax Bay, Russky Island, Vladivostok, 690922, Russian Federation), **SPIN-code: 1668-0742**, **ORCID ID: 0000-0003-3908-4160**, **Scopus Author ID: 57194423783**, **ResearcherID: X-1355-2019**, tefimova@ibss-ras.ru

Pavel A. Salyuk, Head of Laboratory, Laboratory of Satellite Oceanology and Laser Sensing, V. I. Il'ichev Pacific Oceanological Institute, Far Eastern Branch of Russian Academy of Sciences (43 Baltiyskaya Str., Vladivostok, 690041, Russian Federation), CSc. (Phys.-Math.), **SPIN-code: 1454-3891**, **ORCID ID: 0000-0002-3224-710X**, **Scopus Author ID: 9737122900**, **ResearcherID: E-8592-2014**, pavel.salyuk@gmail.com

Andrey V. Yatsuk, Leading Researcher, International Scientific Centre for Ecology and Climate Change, Sirius University of Science and Technology (1 Olympic Ave., Federal Territory "Sirius", 354340, Russian Federation), Csc. (Geol.), **SPIN-code: 5704-5884**, **ORCID ID: 0000-0003-3975-5438**, **Scopus Author ID: 55189937800**, **ResearcherID: I-3720-2017**, yatsuk.av@talantiuspeh.ru

Contribution of the co-authors:

Tatyana Ya. Churilova – conceived the study, developed the research methodology, conducted the investigation, and prepared the original draft of the manuscript

Elena Yu. Skorokhod – organised and curated the research data and prepared visual presentation of the results

Natalia A. Moiseeva – organised and curated the research data and prepared visual presentation of the results

Anatoly S. Buchelnikov – developed and implemented the software used for data processing and contributed to the visualisation of the results

Tatyana V. Efimova – validated the data and verified the accuracy and reliability of the results

Pavel A. Salyuk – performed formal analysis of the data

Andrey V. Yatsuk – organised and curated the research data

The authors have read and approved the final manuscript.
The authors declare that they have no conflict of interest.

Supplement 1

Values of spectral coefficients obtained for the relationship between $a_{ph}(\lambda)$ and *TChl-a* described by the power equation $a_{ph}(\lambda) = A(\lambda)\cdot(TChl\text{-}a)^{B(\lambda)}$ for the upper mixed layer (UML); determination coefficient (r^2)

λ, nm	$A(\lambda)$	$B(\lambda)$	r^2	λ, nm	$A(\lambda)$	$B(\lambda)$	r^2
400	0.038	0.702	0.775	402	0.040	0.700	0.776
404	0.041	0.699	0.781	406	0.042	0.696	0.787
408	0.044	0.694	0.788	410	0.045	0.692	0.796
412	0.047	0.690	0.798	414	0.048	0.687	0.800
416	0.049	0.684	0.803	418	0.050	0.683	0.804
420	0.051	0.683	0.807	422	0.051	0.691	0.802
424	0.052	0.683	0.798	426	0.053	0.682	0.802
428	0.054	0.685	0.808	430	0.055	0.684	0.809
432	0.056	0.688	0.815	434	0.057	0.687	0.813
436	0.058	0.687	0.814	438	0.059	0.684	0.811
440	0.058	0.685	0.812	442	0.058	0.682	0.811
444	0.056	0.684	0.810	446	0.055	0.680	0.804
448	0.054	0.680	0.801	450	0.053	0.678	0.794
452	0.052	0.679	0.792	454	0.052	0.677	0.787
456	0.051	0.679	0.788	458	0.051	0.677	0.785
460	0.051	0.676	0.784	462	0.051	0.675	0.782
464	0.051	0.675	0.781	466	0.051	0.670	0.775
468	0.050	0.667	0.770	470	0.050	0.665	0.766
472	0.049	0.660	0.760	474	0.048	0.659	0.757
476	0.047	0.656	0.752	478	0.046	0.656	0.752
480	0.045	0.655	0.751	482	0.043	0.659	0.758
484	0.042	0.664	0.763	486	0.041	0.669	0.771
488	0.039	0.680	0.784	490	0.038	0.688	0.792
492	0.036	0.701	0.803	494	0.035	0.713	0.813
496	0.033	0.726	0.821	498	0.031	0.740	0.830
500	0.029	0.751	0.834	502	0.028	0.763	0.840
504	0.026	0.777	0.846	506	0.024	0.789	0.850
508	0.023	0.799	0.851	510	0.022	0.809	0.853
512	0.021	0.821	0.857	514	0.019	0.831	0.860
516	0.018	0.839	0.861	518	0.018	0.848	0.864
520	0.017	0.859	0.867	522	0.016	0.867	0.870
524	0.015	0.876	0.871	526	0.015	0.883	0.874
528	0.014	0.890	0.877	530	0.013	0.898	0.880
532	0.013	0.903	0.882	534	0.012	0.908	0.885
536	0.012	0.912	0.887	538	0.011	0.916	0.888
540	0.011	0.919	0.891	542	0.010	0.923	0.894
544	0.010	0.926	0.895	546	0.009	0.930	0.897

Table concluded

λ, nm	*A*(λ)	*B*(λ)	r^2	λ, nm	*A*(λ)	*B*(λ)	r^2
548	0.009	0.931	0.897	550	0.009	0.935	0.898
552	0.008	0.937	0.899	554	0.008	0.941	0.899
556	0.007	0.944	0.900	558	0.007	0.946	0.899
560	0.006	0.947	0.897	562	0.006	0.956	0.899
564	0.006	0.954	0.894	566	0.005	0.955	0.892
568	0.005	0.955	0.889	570	0.005	0.953	0.888
572	0.005	0.954	0.884	574	0.005	0.954	0.882
576	0.005	0.953	0.880	578	0.005	0.950	0.875
580	0.005	0.950	0.872	582	0.005	0.943	0.867
584	0.005	0.940	0.861	586	0.005	0.936	0.856
588	0.005	0.929	0.848	590	0.005	0.924	0.841
592	0.005	0.918	0.835	594	0.005	0.914	0.830
596	0.005	0.908	0.829	598	0.005	0.900	0.826
600	0.005	0.896	0.830	602	0.005	0.893	0.836
604	0.005	0.893	0.841	606	0.005	0.894	0.851
608	0.005	0.900	0.861	610	0.005	0.905	0.871
612	0.005	0.910	0.875	614	0.005	0.916	0.884
616	0.005	0.922	0.892	618	0.005	0.926	0.896
620	0.005	0.927	0.901	622	0.006	0.927	0.903
624	0.006	0.928	0.905	626	0.006	0.929	0.903
628	0.006	0.927	0.901	630	0.006	0.921	0.900
632	0.006	0.914	0.901	634	0.007	0.903	0.898
636	0.007	0.894	0.894	638	0.007	0.879	0.890
640	0.007	0.867	0.883	642	0.007	0.849	0.877
644	0.007	0.833	0.872	646	0.008	0.821	0.869
648	0.008	0.814	0.876	650	0.008	0.817	0.884
652	0.008	0.829	0.892	654	0.008	0.840	0.895
656	0.008	0.854	0.896	658	0.009	0.859	0.891
660	0.011	0.861	0.889	662	0.013	0.855	0.888
664	0.015	0.851	0.890	666	0.017	0.846	0.894
668	0.019	0.844	0.900	670	0.021	0.843	0.906
672	0.023	0.844	0.913	674	0.023	0.847	0.920
676	0.023	0.852	0.926	678	0.022	0.860	0.931
680	0.020	0.870	0.935	682	0.017	0.894	0.938
684	0.014	0.924	0.939	686	0.011	0.958	0.936
688	0.008	0.999	0.921	690	0.006	1.038	0.896
692	0.004	1.070	0.858	694	0.003	1.087	0.819
696	0.002	1.092	0.788	698	0.002	1.081	0.761
700	0.001	1.060	0.751				

Supplement 2

Values of spectral coefficients obtained for the relationship between $a_{ph}(\lambda)$ and *TChl-a* described by the power equation $a_{ph}(\lambda) = A(\lambda)\cdot(TChl\text{-}a)^{B(\lambda)}$ for the layer Z_{UML} – optical depth 4.6; determination coefficient (r^2)

λ, nm	*A*(λ)	*B*(λ)	r^2	λ, nm	*A*(λ)	*B*(λ)	r^2
400	0.032	0.740	0.834	402	0.033	0.732	0.827
404	0.034	0.731	0.830	406	0.035	0.729	0.825
408	0.037	0.726	0.822	410	0.038	0.728	0.822
412	0.039	0.721	0.816	414	0.040	0.719	0.815
416	0.041	0.717	0.812	418	0.041	0.715	0.811
420	0.042	0.713	0.808	422	0.042	0.721	0.812
424	0.042	0.721	0.810	426	0.043	0.720	0.807
428	0.044	0.719	0.801	430	0.045	0.721	0.798
432	0.046	0.717	0.791	434	0.047	0.719	0.791
436	0.047	0.717	0.784	438	0.048	0.714	0.782
440	0.047	0.718	0.781	442	0.047	0.715	0.781
444	0.046	0.709	0.775	446	0.046	0.705	0.773
448	0.045	0.702	0.768	450	0.044	0.703	0.767
452	0.044	0.699	0.762	454	0.043	0.697	0.760
456	0.043	0.698	0.760	458	0.043	0.692	0.755
460	0.043	0.692	0.755	462	0.043	0.689	0.752
464	0.044	0.684	0.746	466	0.044	0.679	0.741
468	0.043	0.676	0.738	470	0.043	0.670	0.731
472	0.043	0.666	0.728	474	0.042	0.660	0.722
476	0.041	0.657	0.721	478	0.040	0.658	0.721
480	0.039	0.656	0.721	482	0.038	0.660	0.726
484	0.037	0.664	0.731	486	0.036	0.670	0.738
488	0.035	0.677	0.748	490	0.034	0.684	0.755
492	0.032	0.693	0.764	494	0.031	0.703	0.772
496	0.030	0.712	0.780	498	0.028	0.721	0.787
500	0.027	0.729	0.794	502	0.026	0.738	0.802
504	0.025	0.744	0.807	506	0.024	0.750	0.812
508	0.022	0.758	0.818	510	0.022	0.762	0.822
512	0.021	0.770	0.828	514	0.020	0.776	0.834
516	0.019	0.780	0.838	518	0.018	0.785	0.844
520	0.018	0.792	0.849	522	0.017	0.796	0.853
524	0.016	0.801	0.858	526	0.016	0.809	0.863
528	0.015	0.813	0.869	530	0.015	0.821	0.874
532	0.014	0.826	0.879	534	0.013	0.829	0.884
536	0.013	0.835	0.886	538	0.012	0.836	0.890
540	0.012	0.842	0.894	542	0.011	0.846	0.895
544	0.011	0.849	0.897	546	0.010	0.856	0.898

Table concluded

λ, nm	$A(\lambda)$	$B(\lambda)$	r^2	λ, nm	$A(\lambda)$	$B(\lambda)$	r^2
548	0.010	0.857	0.898	550	0.009	0.860	0.897
552	0.009	0.864	0.896	554	0.009	0.865	0.895
556	0.008	0.868	0.895	558	0.008	0.873	0.893
560	0.007	0.873	0.888	562	0.007	0.872	0.889
564	0.007	0.870	0.887	566	0.006	0.868	0.882
568	0.006	0.865	0.878	570	0.006	0.859	0.874
572	0.006	0.857	0.865	574	0.006	0.860	0.864
576	0.006	0.858	0.858	578	0.006	0.859	0.849
580	0.006	0.859	0.846	582	0.005	0.859	0.840
584	0.006	0.853	0.830	586	0.006	0.854	0.824
588	0.006	0.848	0.811	590	0.006	0.845	0.802
592	0.006	0.841	0.795	594	0.005	0.839	0.792
596	0.005	0.835	0.794	598	0.005	0.832	0.797
600	0.005	0.833	0.806	602	0.005	0.830	0.815
604	0.005	0.831	0.825	606	0.005	0.839	0.840
608	0.005	0.842	0.849	610	0.005	0.849	0.860
612	0.005	0.856	0.870	614	0.005	0.864	0.878
616	0.005	0.870	0.884	618	0.006	0.874	0.890
620	0.006	0.878	0.894	622	0.006	0.882	0.897
624	0.006	0.881	0.897	626	0.006	0.884	0.896
628	0.006	0.880	0.893	630	0.006	0.875	0.890
632	0.006	0.864	0.891	634	0.007	0.857	0.889
636	0.007	0.849	0.889	638	0.007	0.842	0.885
640	0.007	0.835	0.881	642	0.007	0.823	0.877
644	0.007	0.813	0.877	646	0.007	0.809	0.883
648	0.007	0.808	0.889	650	0.007	0.812	0.897
652	0.007	0.824	0.901	654	0.008	0.832	0.898
656	0.008	0.841	0.893	658	0.009	0.844	0.886
660	0.011	0.837	0.879	662	0.013	0.828	0.879
664	0.015	0.817	0.880	666	0.017	0.810	0.887
668	0.019	0.806	0.897	670	0.021	0.804	0.907
672	0.022	0.808	0.915	674	0.022	0.816	0.919
676	0.022	0.827	0.918	678	0.020	0.842	0.914
680	0.018	0.860	0.908	682	0.016	0.884	0.902
684	0.013	0.920	0.894	686	0.010	0.959	0.883
688	0.007	1.010	0.868	690	0.005	1.062	0.845
692	0.004	1.108	0.812	694	0.003	1.133	0.786
696	0.002	1.126	0.760	698	0.002	1.092	0.745
700	0.002	1.041	0.729				